J. Min. Metall. Sect. B-Metall. 48 (3) B (2012) 367 - 374

Journal of Mining and Metallurgy, Section B: Metallurgy

INVESTIGATION OF THE ISOTHERMAL SECTION AT 1000°C IN THE Pt–Al–Cr SYSTEM

R. Süss[a,b,c,*], L.A. Cornish[b,c], M.J. Witcomb[b,d]

[a] Advanced Materials Division, Mintek, Randburg, South Africa.
[b] DST/NRF Centre of Excellence in Strong Materials, University of the Witwatersrand, WITS, South Africa.
[c] School of Chemical and Metallurgical Engineering, University of the Witwatersrand, WITS, South Africa.
[d] Microscopy and Microanalysis Unit, University of the Witwatersrand, WITS, South Africa.

(Received 03 May 2012; accepted 25 October 2012)

Abstract

Platinum-based alloys are being developed with γ/γ′ microstructures analogous to nickel-based superalloys, with potential for high temperature applications. The ternary Pt-Al-Cr system was investigated to provide data for the continued development of a thermodynamic database for the Pt-Al-Cr-Ru system. The alloys were studied in the 1000°C annealed and quenched conditions, using SEM with EDX and XRD. Isothermal sections were constructed.

Keywords: *Microstructure; Ternary Phase Diagram; Isothermal Section.*

1. Introduction

Platinum-based alloys are being developed with γ/γ′ microstructures analogous to nickel-based superalloys [1, 2]. Although the use of Pt-based alloys as a replacement for Ni-based superalloys is limited because of their higher price and higher density, they have the potential for application in critical components, or as corrosion resistant coatings. The necessity for a predictive thermodynamic database for Pt-containing alloys was identified in the beginning of the Mintek alloy development programme, and it was envisaged that, similar for the NBSAs, the high-temperature Pt-alloys would contain at least 5 components, but as a first stage in the database construction, the major components needed to be identified. Experimental studies of the microstructure and mechanical and oxidation properties showed that a thermodynamic database for the development of Pt-alloys for high-temperature applications should be based on Pt-Al-Cr-Ru [3, 4]. The information needed for the computer assessments was either gleaned from literature, or when not available or contradictory, undertaken within the project. Experimental studies of the four component ternary systems have been undertaken for Al-Cr-Ru [5-8], Pt-Cr-Ru [9-11] and Pt-Al-Ru [12, 13]. This paper summarises results obtained from experimental work on annealed Pt–Al–Cr alloys.

2. Previous work

The work that has been done earlier by other authors on the binary systems that constitute Pt–Al–Cr has already been summarised [14]. A partial ternary isothermal section of the Pt-Al-Cr system at 1350°C was determined by Hill et al. [15,16]. The Pt_3Al phase field was significantly increased by the addition of Cr compared to its width in the binary system. The single-phase ~Pt_3Al and (Pt) phases were shown, but their phase boundaries were not accurately determined above 30 at.% Cr because it was of no interest to that particular investigation. This paper follows on from the determination of a solidification and liquidus surface projection by studying as-cast samples in the Pt-Al-Cr system [14, 17].

3. Experimental procedure

The alloys were prepared by arc-melting the pure (at least 99.9%) elements under an argon atmosphere. This was repeated twice to achieve mixing. These as-cast samples were then cut in half with an Accutom® cutting wheel, and prepared metallographically. After examination of the as-cast microstructures [14], one half of the samples were annealed at 1000°C for 1000 h. The samples were annealed in air and subsequently quenched in water. After annealing, all the samples were polished using an oxide polishing (OP-S) system. The microstructure was examined using a JEOL JSM-840 scanning electron microscope (SEM)

* *Corresponding author: rainer.suss@gmail.com*

DOI:10.2298/JMMB120503046S

Dedicated to the memory of Professor Zbigniew Moser

at 20 kV and the phases and overall composition of the samples were analysed using a Noran energy dispersive X-ray spectroscopy (EDX) system (with standards), using Vantage software. Samples were usually imaged in the backscattered electron (BSE) imaging mode. In a few cases, fine porosity were analysed using a Cameca SX50 Microprobe. To identify the phases, X-ray diffraction (XRD) analyses were conducted on the polished samples using a Siemens D500 diffractometer with Mo Kα radiation. Peaks were compared with the JCPDS database [18], or with simulations using Crystallographica (available from Oxford Cryosystems) [19].

No access to powder XRD was available and remelting would probably have changed the compositions and so was not done. Any alloys that were likely to experience melting at 1000°C were not annealed. Except for alloy $Pt_{10}:Al_{80}:Cr_{10}$, none of the alloys that could form L + ~Pt_8Al_{21}/~$CrAl_4$/~$CrAl_5$ or any other Al-rich compounds, were annealed at 1000°C.

4. Results

All compositions are quoted in at.%, and the overall sample and phase compositions are given in Table 1. Section and table titles refer to nominal (target) values. All phases were confirmed by XRD unless otherwise stated.

4.1. (1) $Pt_3:Al_{35}:Cr_{62}$

After annealing, alloy $Pt_3:Al_{35}:Cr_{62}$ showed rounded (Cr) dendrites with grey particles inside that had coarsened during annealing compared to the as-cast structure [14]. Between the (Cr) was a fine eutectic mixture of (Cr) and ~$PtAl_2$ which had lost most of its as-cast cellular morphology (Fig. 1). XRD analyses could not be performed on the sample since it crumbled during the procedure of breaking it out of its mount after SEM analyses. The identity of ~$PtAl_2$ was in agreement with Alloys $Pt_{30}:Al_{50}:Cr_{20}$ and $Pt_{35}:Al_{55}:Cr_{10}$. The composition of the black + grey and its resulting position on the Gibbs triangle suggests a position for the grey phase near that of ~Cr_2Al or even τ_2»Cr_3Al_2, although ~Cr_2Al is only stable up to 910°C according to the Al-Cr phase diagram [20].

4.2. (2) $Pt_3:Al_{65}:Cr_{32}$

During annealing, the dendritic structure of as-cast $Pt_3:Al_{65}:Cr_{32}$ disappeared, as well as the eutectic mixture. The result was an alloy that comprised small areas of ~$PtAl_2$ in a ~Cr_4Al_9 matrix (Fig. 2). These major changes in the microstructure show that the melting ranges were fairly near the annealing temperature since diffusion was effective.

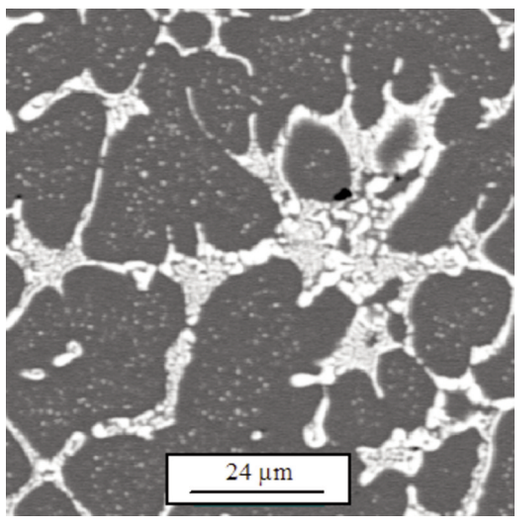

Figure 1. *BSE-SEM image of nominal $Pt_3:Al_{35}:Cr_{62}$ (Alloy 1) after annealing at 1000°C: (Cr) dark; ~$PtAl_2$ light; ~Cr_2Al/τ_2»Cr_3Al_2 medium.*

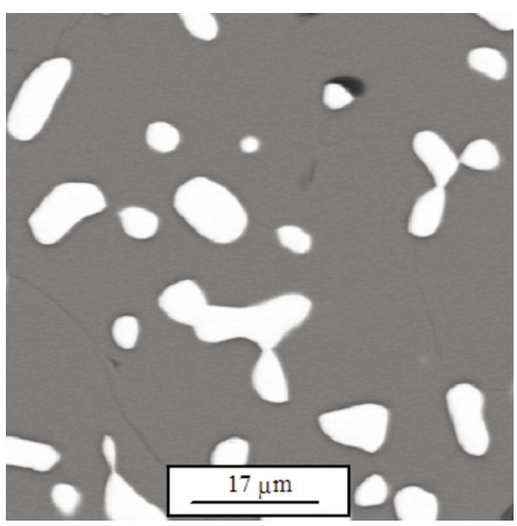

Figure 2. *BSE-SEM image of nominal $Pt_3:Al_{65}:Cr_{32}$ (Alloy 2) after annealing at 1000°C: ~Cr_4Al_9 dark; ~$PtAl_2$ light.*

4.3. (8) $Pt_{10}:Al_{30}:Cr_{60}$

Very similar in appearance to its structure in the as-cast condition, alloy $Pt_{10}:Al_{30}:Cr_{60}$ comprised remnants of (Cr) dendrites, with a eutectic mixture of (Cr) and ~$PtAl_2$ that had become more sparse and coarsened during annealing at 1000°C (Fig. 3). It was even clearer in the annealed sample that ~Cr_2Al precipitates were present inside the (Cr) phase and therefore stable at 1000°C, indicating that it was stable at higher temperatures in the ternary than in the binary system.

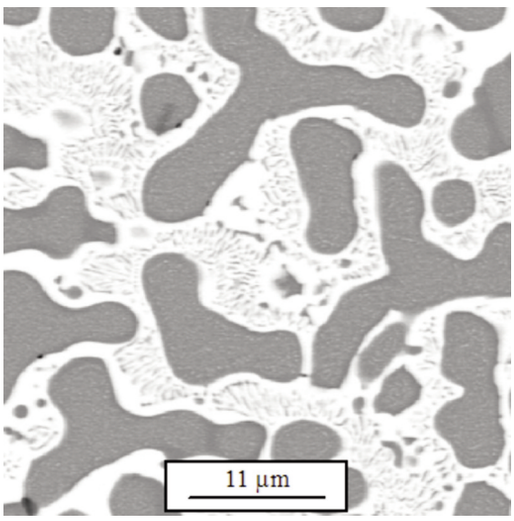

Figure 3. *BSE-SEM image of nominal $Pt_{10}:Al_{30}:Cr_{60}$ (Alloy 8) after annealing at 1000°C: (Cr) dark; ~$PtAl_2$ white; ~Cr_2Al light precipitates.*

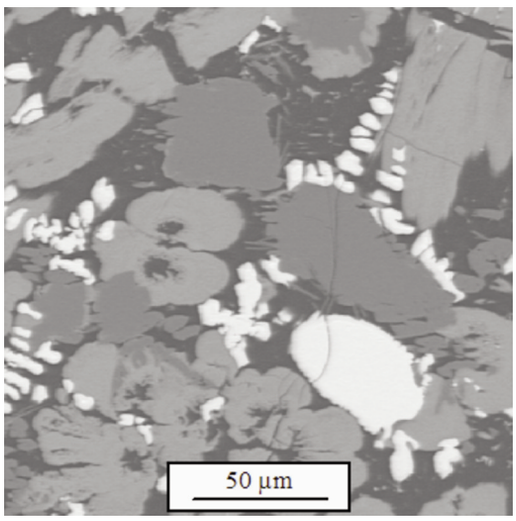

Figure 4. *BSE-SEM image of nominal $Pt_{10}:Al_{80}:Cr_{10}$ (Alloy 11) after annealing at 1000°C: (Al) very dark and dark medium; ~$CrAl_3$ light medium; ~$PtAl_2$ white (chunky); ~Pt_8Al_{21} white (dendritic).*

4.4. (11) $Pt_{10}:Al_{80}:Cr_{10}$

In the as-cast condition, alloy $Pt_{10}:Al_{80}:Cr_{10}$ had a very complicated structure, comprising four phases. Its appearance changed considerably during annealing with the phases becoming much rounder compared to their more angular appearance in the as-cast condition, and the ~$PtAl_2$ phase was much larger and easier to analyse after annealing (Fig. 4). There was also much porosity present (not shown), as well as cracks, indicating brittleness, or at least different coefficients of expansion for the phases. Most of the phases had changed compositions, and the (Al) and ~$PtAl_2$ showed decreased solubility for the components. The two areas with the darkest contrast had almost identical compositions (Table 1) and were deduced to be both (Al). The reason for their difference in contrast and morphology with distinct interfaces was not clear, although it could be an orientation effect of resolidified areas. The areas of lightest contrast also comprised two phases of distinctly different morphologies (chunky vs. dendritic). These could not be differentiated by EDX, and XRD only detected ~$PtAl_2$, but the as-cast results indicated that the other phase was ~Pt_8Al_{21} [14]. The alloy composition relative to the liquid stability range in the Pt-Al and Al-Cr systems, and the fact that the phases did become much rounder and ~$PtAl_2$ appeared dendritic, suggested that some liquation have occurred or the annealing temperature was very close to the liquidus to allow much diffusion. This was highly likely at 1000°C. Therefore, the results of this alloy suggest a liquid boundary at 1000°C as indicated by the dashed line in Fig. 13.

4.5. (14) $Pt_{15}:Al_5:Cr_{80}$

At lower magnification, alloy $Pt_{15}:Al_5:Cr_{80}$ appeared similar to its as-cast state in the fact that it comprised areas (previously dendrites) surrounded by a eutectic mixture. Higher magnification revealed that the dark former dendritic areas were in fact two-phase mixtures (Fig. 5). Although the phases were too fine for accurate analysis, XRD confirmed that it comprised (Cr) and ~Cr_3Pt (which had precipitated during annealing). The now much coarsened eutectic mixture consisted of ~Cr_3Pt (which had been ~CrPt in the as-cast state [14]). This was consistent with the results of Alloys $Pt_{18}:Al_2:Cr_{80}$ and $Pt_{38}:Al_{22}:Cr_{40}$.

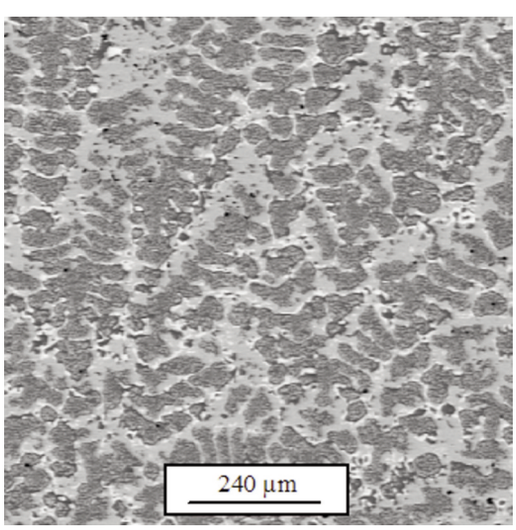

Figure 5. *BSE-SEM image of nominal $Pt_{15}:Al_5:Cr_{80}$ (Alloy 14) after annealing at 1000°C: (Cr) dark; ~Cr_3Pt medium; ~PtAl white.*

4.6. (16) $Pt_{18}:Al_2:Cr_{80}$

Alloy $Pt_{18}:Al_2:Cr_{80}$ comprised three phases: (Cr), ~Cr_3Pt and τ_1 (Fig. 6). Its general appearance was similar to that of its as-cast state [14], except that the amount of (Cr) and τ_1 (transformed from ~CrPt during annealing) had decreased substantially, while some ~Cr_3Pt had precipitated inside the (Cr) due to the strong decrease of solubility of Pt in (Cr) as seen in the binary system [19]. Since the dendritic structure of the alloy was still intact, it is assumed that alloy had not reached equilibrium yet. Assuming that it is likely that the amount of (Cr) and τ_1 will continue to decrease, it is possible they might fully disappear on further annealing, or only a very small volume percentage will remain (the overall composition of the alloy and that of ~Cr_3Pt was already very similar).

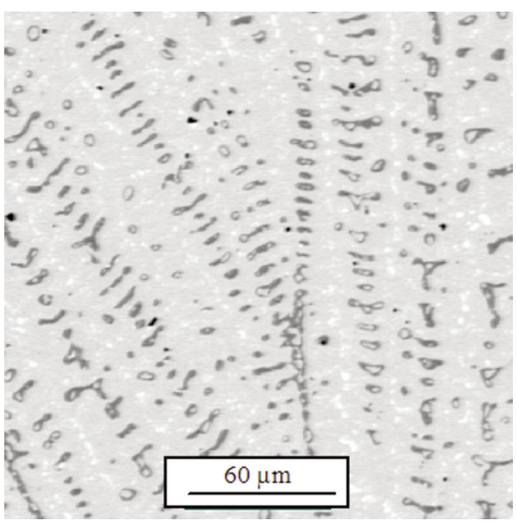

Figure 6. *BSE-SEM image of nominal $Pt_{18}:Al_2:Cr_{80}$ (Alloy 16) after annealing at 1000°C: (Cr) dark; ~Cr_3Pt medium; τ_1 white.*

4.7. (21) $Pt_{30}:Al_{50}:Cr_{20}$

Alloy $Pt_{30}:Al_{50}:Cr_{20}$ comprised primarily ~$PtAl_2$ dendrites with ~Pt_2Al_3 Widmanstätten needles, and interdendritic regions that comprised a mixture of ~$PtAl_2$ + (Cr) + ~Pt_2Al_3 (not ~PtAl as in the as-cast state [14]) (Fig. 7(a)). There was also evidence of (Cr) precipitates within the ~$PtAl_2$ phase (Fig. 7(b)). The interdendritic mixture of phases had become uniform and coarser during annealing while Widmanstätten needles had formed inside the dendrites. In many cases, the black areas were holes. Analysis under the microprobe confirmed (Cr), and no oxygen, being at the bottom of all the holes analysed, and it is thus assumed that the holes were not originally filled with oxides, but with (Cr) which had been pulled out during polishing.

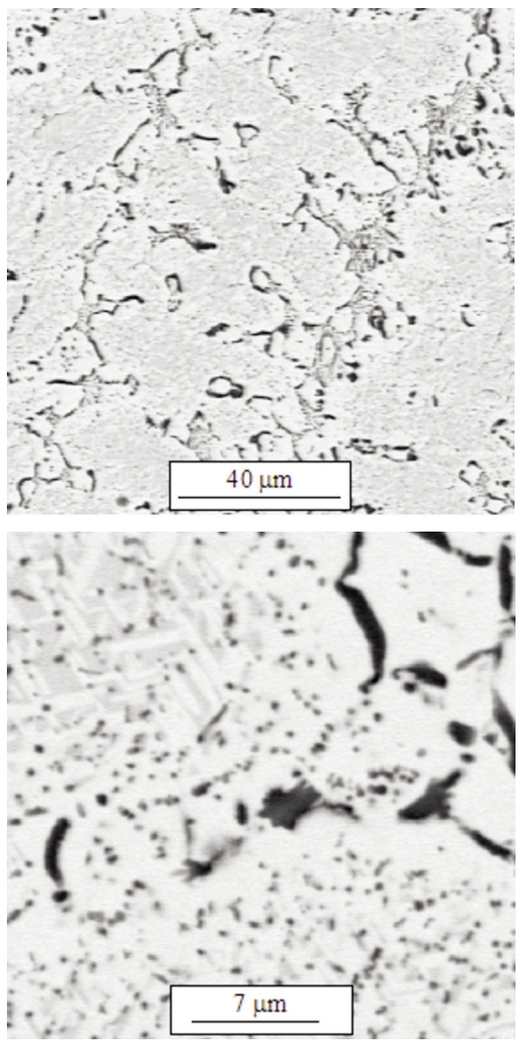

Figure 7. *(a). BSE-SEM image of nominal $Pt_{30}:Al_{50}:Cr_{20}$ (Alloy 21) after annealing at 1000°C: (Cr) dark; ~$PtAl_2$ medium; ~ Pt_2Al_3 white; (b) Higher magnification of interdendritic region.*

4.8. (23) $Pt_{34}:Al_{49}:Cr_{17}$

As in the as-cast condition, alloy $Pt_{34}:Al_{49}:Cr_{17}$ comprised ~Pt_2Al_3 dendrites (transformed from ~$PtAl_2$) in an interdendritic mixture of (Cr), ~PtAl and ~Pt_2Al_3 (Fig. 8). The alloy was similar in appearance to Alloys $Pt_{35}:Al_{55}:Cr_{10}$ and $Pt_{30}:Al_{50}:Cr_{20}$. Unfortunately, XRD analyses could not be performed on the sample since it crumbled during the procedure of breaking it out of its mount after SEM analyses. The small black spots were confirmed by both SEM and microprobe to be a metallic phase, and not porosity or an oxide. Although too small for accurate measurement, its primary constituent, Cr, was confirmed. The identity of the phases agreed with the assessment for Alloys $Pt_{43}:Al_{52}:Cr_5$, $Pt_{35}:Al_{55}:Cr_{10}$ and $Pt_{30}:Al_{50}:Cr_{20}$. The general morphology had not

changed much, showing that the alloy's melting point was much higher than 1000°C and limited diffusion had taken place. Close examination of the dendrites suggested the presence of a second phase, possibly remnants of ~$PtAl_2$. The EDX analysis given in Table 1 for Pt_2Al_3 would be a two-phase analysis (explaining the large errors in the EDX results), and would also explain the high Cr content compared to those of Alloys Pt_{30}:$Al_{50}Cr_{20}$ and Pt_{35}:$Al_{55}Cr_{10}$.

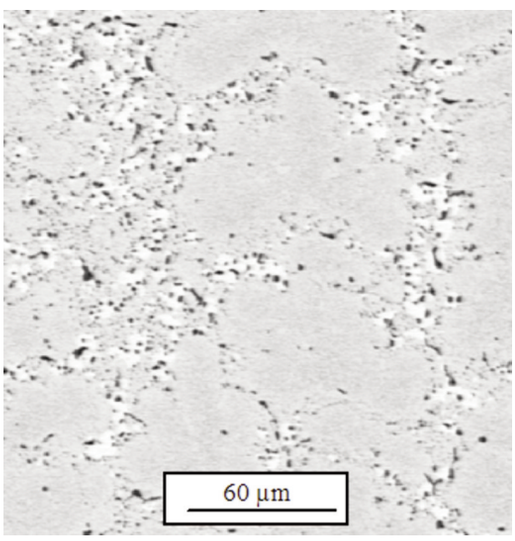

Figure 8. *BSE-SEM image of nominal Pt_{34}:Al_{49}:Cr_{17} (Alloy 23) after annealing at 1000°C: (Cr) black; ~Pt_2Al_3 + ~$PtAl_2$ medium; ~PtAl white.*

4.9. (24) Pt_{35}:Al_{55}:Cr_{10}

At low magnification, alloy Pt_{35}:Al_{55}:Cr_{10} comprised mostly columnar ~$PtAl_2$ grains with rims of lighter contrast and black porosity on the grain boundaries (Fig. 9(a)). This was very different to the alloy's appearance in the as-cast state [14]. At higher magnification, ~Pt_2Al_3 needles were seen inside the ~$PtAl_2$ grains (Fig. 9(b)), as well as a difficult-to-distinguish phase mixture at grain junctions (Fig. 9(c)). The assessment concurred with that of alloy Pt_{30}:Al_{50}:Cr_{20}.

4.10. (26) Pt_{38}:Al_{22}:Cr_{40}

During annealing at 1000°C, the dendritic structure of alloy Pt_{38}:Al_{22}:Cr_{40} changed dramatically to (Cr) and ~Cr_3Pt dispersed in a τ_1 matrix (Fig. 10). The identities of the phases were in agreement with alloy Pt_{18}:Al_2:Cr_{80}. Interestingly the composition of the major τ_1 phase had not changed significantly during annealing.

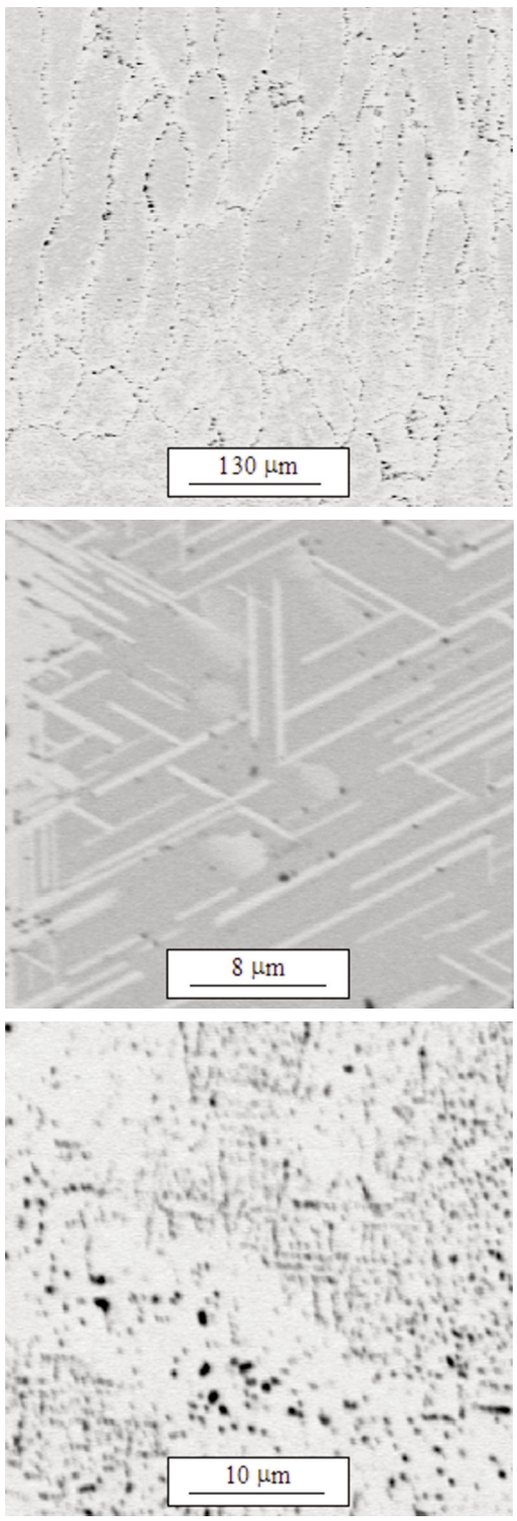

Figure 9. *(a). BSE-SEM image of nominal Pt_{35}:Al_{55}:Cr_{10} (Alloy 24) after annealing at 1000°C: (Cr) dark; ~$PtAl_2$ medium; ~Pt_2Al_3 light; (b) Higher magnification of ~Pt_2Al_3 needles inside ~$PtAl_2$ grains; (c) Higher magnification of grain junctions.*

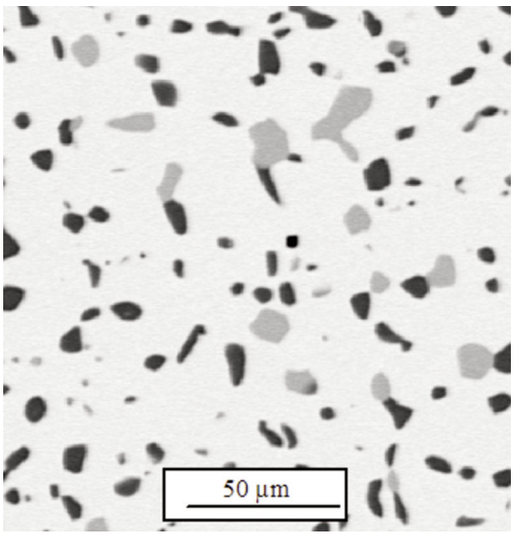

Figure 10. *BSE-SEM image of nominal $Pt_{38}:Al_{22}:Cr_{40}$ (Alloy 26) after annealing at 1000°C: (Cr) dark; ~Cr_3Pt medium; τ_1 light.*

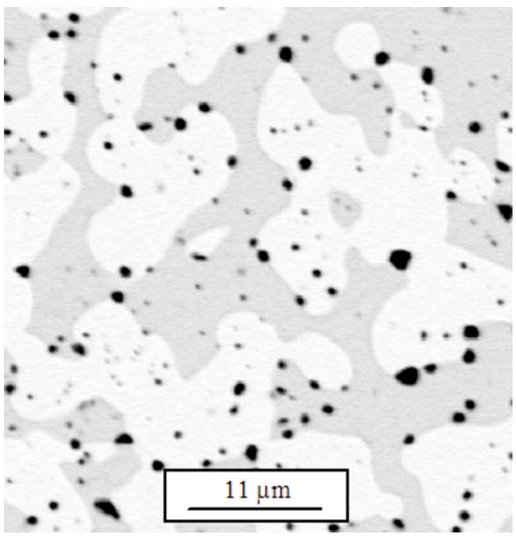

Figure 11. *BSE-SEM image of nominal $Pt_{43}:Al_{52}:Cr_5$ (Alloy 30) after annealing at 1000°C: Pores/(Cr) black; ~ Pt_2Al_3 dark; ~PtAl light.*

4.11. (30) $Pt_{43}:Al_{52}:Cr_5$

Although still comprising two phases (Fig. 11), the appearance of the microstructure of alloy $Pt_{43}:Al_{52}:Cr_5$ changed significantly during annealing: the phases became much coarser and many more pores were present. Unfortunately XRD analyses could not be performed on the sample since it crumbled during the procedure of breaking it out of its mount after SEM analyses, but taking into consideration the EDX measurements and the results of Alloys $Pt_{30}:Al_{50}:Cr_{20}$, $Pt_{35}:Al_{55}:Cr_{10}$ and $Pt_{50}:Al_{35}:Cr_{15}$, the phases were identified as (Cr), ~Pt_2Al_3 and ~PtAl. The melting range had to be close to the annealing temperature since significant diffusion had occurred. This movement of atoms was also responsible for the increased porosity.

4.12. (32) $Pt_{50}:Al_{10}:Cr_{40}$; (33) $Pt_{50}:Al_{35}:Cr_{15}$

Alloy $Pt_{50}:Al_{10}:Cr_{40}$ changed from ~CrPt dendrites in a ~Pt_2Al matrix in the as-cast state [14], to a single-phase ~CrPt alloy during annealing at 1000°C. After annealing at 1000°C, alloy $Pt_{50}:Al_{35}:Cr_{15,}$ clearly had a two-phase structure comprising τ_1 and ~PtAl, compared to the cored single phase τ_1 structure it had in the as-cast state.

4.13. (36) $Pt_{55}:Al_{25}:Cr_{20}$

Alloy $Pt_{55}:Al_{25}:Cr_{20}$ comprised a minority of ~Pt_2Al (LT) in a matrix of τ_1 and $L1_2$ Pt_3Al (HT) needles (Fig. 12). It could be reasoned that the major phase was in fact a single composition and that the morphology was only different due to crystal structural differences after a martensitic-like transformation. However, it appeared like the needles actually ran through the ~Pt_2Al as well, which would eliminate the possibility of a martensitic phase change since it is unlikely that the new phase would be able to have a shear relationship with both phases. Also, the positions of the measured two-phase and single-phase compositions on the Gibbs triangle relative to the overall composition of the alloy clearly indicate the presence of three different phases.

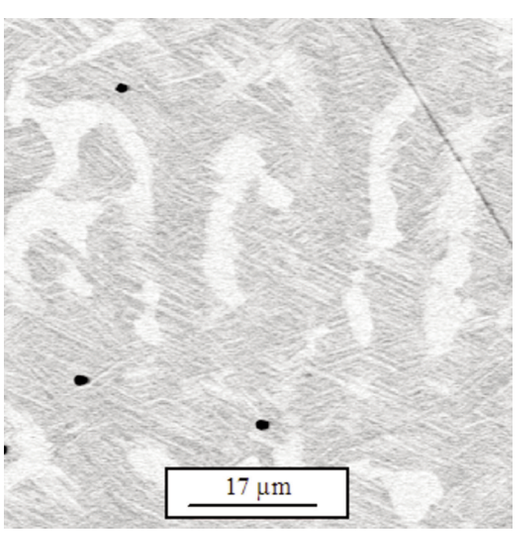

Figure 12. *BSE-SEM image of nominal $Pt_{55}:Al_{25}:Cr_{20}$ (Alloy 36) after annealing at 1000°C: (τ_1 + ~Pt_3Al) dark; ~Pt_2Al white.*

4.14. (37) $Pt_{58}:Al_{10}:Cr_{32}$; (39) $Pt_{63}:Al_{32}:Cr_5$; (41) $Pt_{65}:Al_5:Cr_{30}$

As in the as-cast state, alloy $Pt_{58}:Al_{10}:Cr_{32}$ comprised ~CrPt and $L1_2$ ~Pt_3Al, with the amount of ~Pt_3Al much decreased but easier to distinguish. This would agree with the assessment of Alloys $Pt_{50}:Al_{10}:Cr_{40}$ and $Pt_{50}:Al_{10}:Cr_{40}$.The ~Pt_3Al would probably disappear totally on further annealing. During annealing at 1000°C, the τ_1 phase in alloy $Pt_{63}:Al_{32}:Cr_5$ disappeared, resulting in a single-phase ~Pt_2Al (LT) alloy. The cored appearance of as-cast alloy $Pt_{65}:Al_5:Cr_{30}$ disappeared during annealing to form a clearly single-phase $L1_2$ ~Pt_3Al alloy.

5. Discussion

For easy reference, Fig. 13(a) shows all the actual alloy compositions of Alloys 1 to 42 as measured by EDX (Table 1). Table 2 shows the extension of the phases at 1000°C. Fig. 13(b) shows the 1000°C isothermal section of the Pt-Al-Cr phase diagram, based on the interpretation of the available data. Compared to the solidification projection [14], the phase fields of ~Pt_2Al, ~Pt_2Al_3, ~PtAl and especially τ_1 appeared to have significantly reduced in size due to annealing, which is expected. Tie-lines should not cross in an isothermal section, therefore the ~Cr_3Pt/~PtAl tie-line of alloy 14 ($Pt_{15}:Al_5:Cr_{80}$) that would have cut across those of other alloys, is probably the result of non-equilibrium of that alloy. It indicates that the white ~PtAl phase would probably transform to τ_1, as supported by Alloys 16 and 22 ($Pt_{18}:Al_2:Cr_{80}$ and $Pt_{38}:Al_{22}:Cr_{40}$), or, alternatively, totally disappear. The isothermal section also shows that the structure of laths in alloy 36 ($Pt_{55}:Al_{25}:Cr_{20}$) is unlikely to be a single composition since it would be inconsistent with the rest of the data. The Cr ontent values of Alloys 21 and 24 ($Pt_{30}:Al_{50}Cr_{20}$ and $Pt_{35}:Al_{55}Cr_{10}$) were used for ~Pt_2Al_3 in Fig. 13(b).

Since (Al) would not be stable at 1000°C, and taking into account the highly probable liquation that occurred in alloy $Pt_{10}:Al_{80}:Cr_{10}$, a liquid boundary at 1000°C is suggested as indicated by the dashed line in Fig. 13, based on the results of alloy $Pt_{10}:Al_{80}:Cr_{10}$.

The extension of ~Pt_3Al, ~$PtAl_2$ and ~PtAl has increased after annealing, compared to the solidification projection [14]. This is unusual. The microstructural and XRD evidence also suggest that the slope of the ~Pt_2Al field at 1000°C is dissimilar to that in the solidification projection.

A ~CrPt/(Pt) boundary is shown as a small dashed line in Fig. 13(b) but it does not denote an actual phase boundary. Around this boundary it is still unclear whether ~$CrPt_3$ will order to form ~CrPt at lower temperatures (below ~700°C) or not [20]. None of the alloys that were annealed at 1000°C showed ~$CrPt_3$ or (Pt). If the diagram of Zhao et al. [21] is correct and ~CrPt does not form through (Pt) → ~$CrPt_3$ → ~CrPt (the characterisation of results of as-cast alloys in the Pt-Al-Cr and Pt-Cr-Ru systems seemed to confirm it [10, 11, 14]), the dashed line in Fig. 13(b) simply denotes the estimated position of the ~CrPt/~$CrPt_3$ two-phase region shown by Zhao [21].

In earlier work, a true ternary phase τ_1 was identified for which none of the XRD patterns of the phases in the three binary systems was a good match to its measured pattern [14, 22]. This ternary phase τ_1 was confirmed by similar XRD peaks in this work.

Looking at the diagram, it can be seen that significant areas were covered, and it was concluded that all single-phase and two-phase equilibria were identified correctly because the results were self-consistent. The as-cast samples often showed coring as would be expected from the fast cooling from arc-melting [14]. No coring was present after annealing,

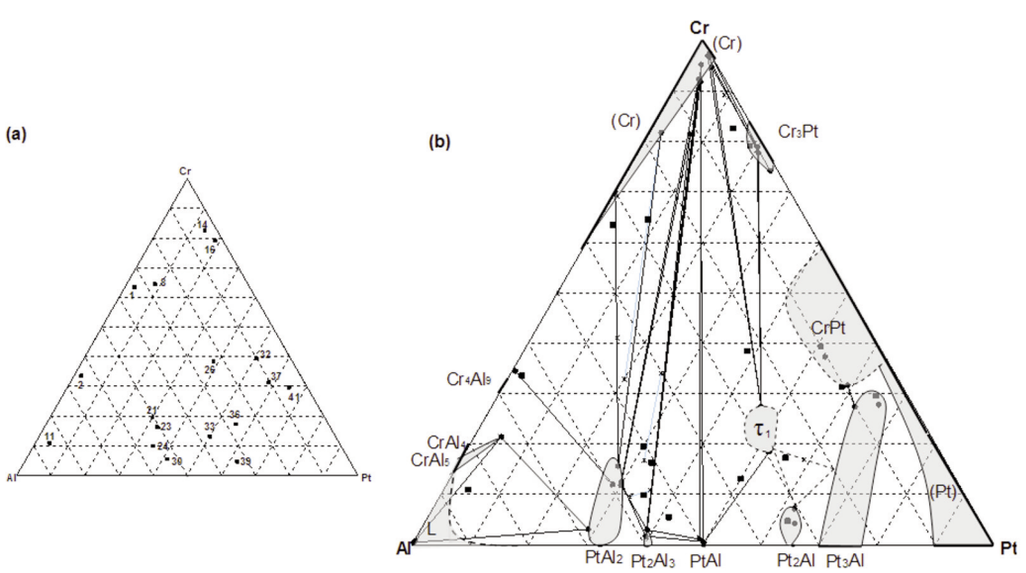

Figure 13. *(a) Alloy numbers and actual compositions of 1000°C annealed samples; (b) 1000°C isothermal section for Pt-Al-Cr.*

and combined with changes in microstructures such as coarsening of phases as well as changes in the phases warrant most of the microstructures as representative of the annealing temperature. Equilibrium or near-equilibrium seemed to have been achieved for most of the annealed samples, and most of the measured compositions of the phases (those that were > 3 μm beam interaction) can be considered as being representative of equilibrium at 1000°C. Sometimes extrapolated values had to be used, either surmised from other alloys, or from the as-cast samples. The interpretation as seen in Fig. 13(b) seems to be the most sensible and the diagrams are self-consistent and reasonably complete.

Since the original completion of this work [23], much of it was confirmed by diffusion multiple method. Using this method developed by Zhao [24], Eastman [25] constructed an isotherm for the Pt-Al-Cr system at 1010°C. Importantly, the ternary phase τ_1 was also confirmed by the alternative methodology. However, there appear to be some discrepancies between Eastman's isotherm and the one given here in Fig. 13(b), particularly with regards to the three-phase regions involving (Cr) and intermetallic phases $PtAl_2$, Pt_2Al_3, PtAl, and Cr_3Pt. Clearly more work is required by both metallographic and diffusion multiple method (or a combination thereof), in order to determine the equilibrium triangles more accurately. Still, a significant amount of information about the Pt-Al-Cr system is now available, which will be of great aid in further thermodynamic modelling.

6. Conclusions

After using SEM with EDX, and XRD on a selection of alloys, the isothermal section at 1000°C was constructed for the Pt-Al-Cr system. Since the results were self-consistent, it is believed that most phase relations have been successfully identified to assist the establishment of a thermodynamic database for the Pt-Al-Cr system.

The extension of the Pt-Al intermetallic compounds (~$PtAl_2$, ~PtAl and especially ~Pt_2Al and ~Pt_3Al) were surprisingly significant, compared to those of the Cr-Al system. A ~20-30% solubility of Cr in was found in most cases except for ~Pt_8Al_{21} and ~Pt_2Al_3. None of the alloys that were annealed at 1000°C showed either ~Pt_3Cr or (Pt) and therefore no ~CrPt/~$CrPt_3$ or ~$CrPt_3$/(Pt) boundaries were drawn. The existence of a true ternary phase τ_1 found in earlier work was confirmed.

Acknowledgements

Mintek, Anglo Platinum, Impala Platinum, Lonmin and the Wits DST/NRF Centre of Excellence in Strong Materials are thanked for their financial support. Mr. B. Joja is thanked for operation of the SEM, and Ms. S. Taylor and Ms. L. Glaner for the XRD scans.

References

[1] L.A. Cornish, R. Süss, A. Douglas, L.H. Chown, L. Glaner, Plat. Met. Rev., 53(1) (2009) 2-10.

[2] A. Douglas, P. J. Hill, T. Murakumo, L. A. Cornish and R. Süss, Plat. Met. Rev., 53(2) (2009) 69-77.

[3] R. Süss, L.A. Cornish, P.J. Hill, J. Hohls, D.N. Compton, in: G.E. Fuchs, A.W. James, T. Gabb, M. McLean, H. Harada (Eds.), Advanced Materials and Processes for Gas Turbines, TMS (The Minerals, Metals and Materials Society), Copper Mountain, CO, USA, September 22–26, 2002, pp. 301–307.

[4] L. A. Cornish, J. Hohls, P. J. Hill, S. Prins, R. Süss and D. N. Compton, J. Min. Metall. Sect. B-Metall., 38 (3–4) (2002) 197.

[5] D.N. Compton, L.A. Cornish, M.J. Witcomb, Microscopy and Microanalysis, Vol. 6, Supplement 2, Springer-Verlag, NY, 2000, pp. 370–371.

[6] D.N. Compton, L.A. Cornish, M.J. Witcomb, J. Alloys Compd., 476 (1-2) (2001) 317–318.

[7] D.N. Compton, L.A. Cornish, M.J. Witcomb, Microscopy and Microanalysis, Vol. 7, Supplement 2, Springer-Verlag, NY, 2001, 1248-1249.

[8] D.N. Compton, Ph.D. Thesis, University of the Witwatersrand, 2002.

[9] R. Süss, M.Sc. Dissertation, University of the Witwatersrand, 2004.

[10] R. Süss, L.A. Cornish, M.J. Witcomb, J. Alloys Compd., 416 (1–2) (2006) 80–92.

[11] R. Süss, L.A. Cornish, M.J. Witcomb, J. Alloys Compd., 457 (1-2) (2008) 310–322.

[12] S.N. Prins, M.Sc. Dissertation, University of Pretoria, 2004.

[13] S.N. Prins, L.A. Cornish, P. Boucher, J. Alloys Compd., 403 (1-2) (2005) 245–252.

[14] R. Süss, L.A. Cornish, M.J. Witcomb, J. Alloys Compd., 490 (2010) 124–144.

[15] P.J. Hill, Ph.D. Thesis, University of the Witwatersrand, 2001.

[16] P.J. Hill, L.A. Cornish, P. Ellis, M.J. Witcomb, J. Alloys Compd., 322 (2001) 166–175.

[17] V. Raghavan, J. Phase. Equilib. Diffus., 32(3) (2011) 243-244.

[18] JCPDS-ICCD, Powder Diffraction File, Joint Committee On Powder Diffraction Standards International Center For Diffraction Data, PA, USA, 2001.

[19] Crystallographica, Version 1.31, Oxford Cryosystems, 1997. www.cryosystems.co.uk.

[20] T.B. Massalski (Ed.), Binary Alloy Phase Diagrams, ASM International, 1990.

[21] J.-C. Zhao, X. Zeng and D. Cahill, Materials Today, October 2005, 28-37.

[22] T.B. Ngwenya, M.Sc. Dissertation, University of the Western Cape, 2007.

[23] R. Süss, Ph.D. Thesis, University of the Witwatersrand, 2008.

[24] J.-C. Zhao, Materials Research Society, 16 (2001) 1565-1578.

[25] C.M. Eastman Jr., M.Sc. Thesis, The Ohio State University, 2011.